Steel and Composite Structures, *Vol. 34, No. 3 (2020) 441-452*
DOI: https://doi.org/10.12989/scs.2020.34.3.441

Investigation on the flexural behavior of an innovative U-shaped steel-concrete composite beam

Maxime Turetta*[1,2,3], Christoph Odenbreit[1], Abdelouahab Khelil[2] and Pierre-Olivier Martin[3]

[1]Faculty of Science, Technology and Communication, University of Luxembourg, L-1359 Luxembourg-Kirchberg, Luxembourg
[2]Université de Lorraine, CNRS, IJL, F-54000 Nancy, France
[3]Research and Valorisation Direction, CTICM – Centre Technique Industriel de la Construction Métallique, F-91190 Saint-Aubin, France

(*Received August 6, 2019, Revised September 27, 2019, Accepted November 4, 2019*)

Abstract. Within the French CIFRE research project COMINO, an innovative type of composite beam was developed for buildings that need fire resistance with no additional supports in construction stage. The developed solution is composed of a steel U-shaped beam acting as a formwork in construction stage for a reinforced concrete part that provides the fire resistance. In the exploitation stage, the steel and the reinforced concrete are acting together as a composite beam. This paper presents the investigation made on the load bearing capacity of this new developed steel-concrete composite section. A full-scale test has been carried out at the Laboratory of Structural Engineering of the University of Luxembourg. The paper presents the configuration of the specimen, the fabrication process and the obtained test results. The beam behaved compositely and exhibited high ductility and bending resistance. The shear connection in the tension zone was effective. The beam failed by a separation between the slab and the beam at high deformations, excessive shear forces conducted to a failure of the stirrups in this zone. The test results are then compared with good agreement to analytical methods of design based on EN 1994 and design guidelines are given.

Keywords: composite beam; U-shaped steel section; connection in tension zone; flexural test; failure mechanism; ultimate bending resistance

1. Introduction

This paper presents the experimental investigation and analytical comparisons made on a new type of U-shaped steel-concrete composite beam. This solution comprises a U-shaped steel beam in which the concrete is cast together with the slab. This provides numerous advantages compared to traditional composite beams (with I-shaped sections) or reinforced concrete (RC) beams. The steel section used as a permanent formwork can avoid any propping system during the construction stage. There is no wait for concrete hardening, reducing the construction delays. The beam is fire resistant due to the longitudinal reinforcement bars (rebars) placed inside the section. These advantages are comparable to composite slim-floor beams (CoSFB) as investigated by Braun *et al*. (2015) but with a downstand beam and a lower amount of steel.

For this type of solution, the composite action, between the external steel and the RC part, increases the load bearing capacity and the ductile behavior like a strengthened RC beam by Fiber-Reinforced Polymer (FRP), Peng and Shi (2004), or by Carbon Fiber-Reinforced Polymer (CFRP), Kim and Aboutaha (2004).

Already in the nineties, Oehlers (1993), Oehlers and Bradford (1995), investigated the behavior of composite profiled beams made of a reinforced concrete beam with steel profiled sheets on its sides. They carried out experimental full-scale beams tests and showed that this type of solution can increase the flexural and shear strength. Uy and Bradford (1995a, b) proceeded further investigations on the ductility of this type of beam by experimental and analytical studies; they underlined a failure mode as a combination of bond-slip and local buckling of the steel sheetings.

Following these investigations, Ahn and Ryu (2007) experimentally studied the flexural strength of C-type and L-type modular composite profiled beams (MPB). The concept consists in the arrangements of external steel modules connected to a concrete part. Ahn and Ryu (2008) improved their solution by reinforcing the bottom of the section by welding plates combined with rebars (MPB-R). Finally, Ryu (2010), studied the behavior of T-section modular composite profiled beams (TMPB) considering the concrete slab as the flange of the T-section in order to improve the ductility of the composite beam.

In the continuity of the developed concepts, recent studies have been carried out on innovative steel-concrete solutions where a U-shaped steel section is filled later with concrete. Liu *et al*. (2017) investigated steel-concrete composite beams with U-shaped steel girders with a shear connection realised through L-shaped members welded to the webs or to the top flanges of the U-shaped beam. They

*Corresponding author, Ph.D.
E-mail: maximeturetta@gmail.com

http://www.techno-press.org/?journal=scs&subpage=6
ISSN: 1229-9367 (Print), 1598-6233 (Online)

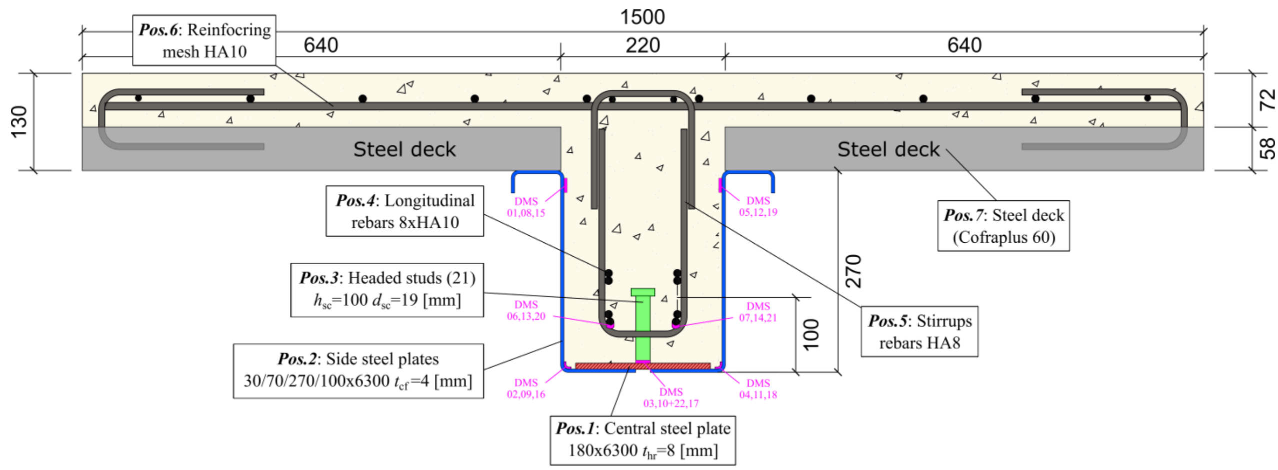

Fig. 1 Details of the composite beam specimen tested with the positions of the strain gauges

(a) Steel decks in the formwork nailed on the U-shaped beam

(b) U-shaped steel section and rebars

Fig. 2 Specimen fabrication before concreting

conducted flexural tests and proposed, for improving ductility and reaching full composite action, to weld the L-shaped on the top flanges or replacing part of them with headed studs.

Keo *et al*. (2018) investigated a similar solution with L-shaped connectors on U-shaped composite beams and conducted push-out tests. They found a high ductility of the shear connection allowing the possibility of full shear interaction. The advantage of these U-shaped solutions with L-shaped connection is that they also prevent the opening of the steel section.

Chen *et al*. (2018) proposed to reduce the number of shear connectors for U-shaped section by increasing the bonding effect with checkered steel plates. Lawson and Taufiq (2019) studied the use of partial shear connection with other types of U-shaped sections with bolts shear connectors. This also underlined the problem of stud welding for light steel plate. The thickness of the steel plates may not be sufficient for welding, thus bolt connectors can avoid this problem. Kozma *et al*. (2019) reviewed different types of bolt connectors and carried out 15 push-out tests in order to evaluate their mechanical behavior.

Additionally, with thin steel plates, the ratio between the thickness and the stud diameter is also limited. In fact, according to Goble (1968), based on 41 specimens tested, for preventing flange pull-out failure, the ratio of the head stud diameter on the steel plate thickness should not exceed 2.7. Common stud diameters between 16 to 19 mm leads to minimal plate thickness between 6 to 7 mm, which is more than the common thickness of light steel plates around 3-4 mm.

Nevertheless, Liu *et al*. (2018) and Zhou *et al*. (2019) presented a novel configuration where the steel U-shaped section, stiffened by a rebar truss on its top flanges, is connected to a reinforced concrete part with welded headed shear stud at the bottom of the section made of cold-formed thin plates (3-4 mm). They found a failure mode by vertical separation from the downstand beam to the concrete slab at the neck and proposed to enhance the integrity of the composite section by adding an inverted U-shaped rebar linking the slab reinforcement to the downstand beam.

Following these very recent developments and their conclusions, a U-shaped steel-concrete composite beam section has been developed with a new arrangement and with the shear connection at the bottom of the section (see Fig. 1). The connection is realised with headed studs welded on a central plate sufficiently thick according to Goble (1968). In order to do so, the U-shaped steel section was made in three parts, with two thin cold-formed side plates and a thicker hot-rolled central plate. Moreover, particular attention has been paid on the disposition of the rebars in particular at the connection between the reinforcing mesh of the slab and the stirrups of the downstand beam.

The paper presents the investigation made on the flexural behavior of this new developed steel-concrete composite section. A full-scale test has been carried out at the Laboratory of Structural Engineering of the University of Luxembourg.

2. Test specimen

2.1 Geometry

The span of the tested composite beam was 6 meters with a total length of 6.3 meters, the beam extended beyond the supports 150 mm each side. The section was a U-shaped steel beam connected to a T-shaped reinforced concrete part as described in Fig. 1.

The U-shaped section was composed of three steel parts assembled together; a hot-rolled steel plate (***Pos.1***) at the bottom and two cold formed steel plates (***Pos.2***) on the sides. The cold-formed plates were folded in an asymmetric Z-shaped section, they constituted the two webs and top flanges of the section. The overall steel section was 270 mm high, 220 mm wide at the bottom and 352 mm wide at the top.

The T-shaped reinforced concrete part was composed of a downstand part and a composite slab. The width of the composite slab (b_{eff}) was equaled to the effective slab width according to EN 1994-1-1 (2005) (see Eq. (1)). The height of the concrete above the steel decking (here Cofraplus60®) was 72 mm. The steel decking (***Pos.7***) were not continuous above the downstand part and were nailed at each ribs on the two top flanges of the steel section. The discontinuity of the steel decking allow the filling with concrete the downstand part at the same time as the slab.

$$b_{\text{eff}} = 2 \times l_{\text{e}} / 8 \tag{1}$$

The composite slab was reinforced with a wire mesh (type ST25C, see $A_{s,slab}$, ***Pos.6***) whereas the downstand part was reinforced with longitudinal rebars (8xHA10, A_s, ***Pos.4***) and stirrups (***Pos.5***). The amount of longitudinal rebars was determined for the fire situation with the required cover (here c=45 mm), as it would be the case for a real use. In order to prevent an uplifting failure between the slab and the downstand beam like found by Liu *et al.* (2018), the stirrups were divided in two U-shaped bended parts (see ***Pos.5*** in Fig. 1). The first part at the bottom linked the longitudinal rebars. The second part connected the reinforcing mesh of the slab to the first part and therefore to the longitudinal rebars.

The shear connection was realised by welding headed studs (***Pos.3***) on the bottom plate. The bottom plate (***Pos.1***) was thicker than the cold-formed plates (***Pos.2***) for two reasons. Firstly, the plate located at the extreme fiber of the section would significantly contribute to the bending resistance of the composite beam. Secondly according to the 42 tests carried out by Goble (1968), the thickness of the steel flange cannot be lower than $0.37d_{sc}$ (were d_{sc} is the diameter of the shear studs, here d_{sc}=19 mm) in order to avoid the pull-out of the headed studs from the steel plate. The main dimensions of the studied steel-concrete composite section are presented in Table 1.

2.2 Material

During the concreting of the composite specimen, 6 concrete cubes and 6 concrete cylinders were prepared. Compression tests were carried out, 34 days later, on the hardened specimens at the laboratory of the University of Luxembourg according to EN 12390-3 (2012). The concrete ordered was a C35/45 with a limit size of the maximal granulates of D_{max}=8 mm with a consistency class F2. The mean measured compression strength was $f_{c,m}$=53 MPa.

After the flexural test, steel coupons were cut out from the composite beam specimen: 9 coupons were cut out in the side cold-formed steel parts (***Pos.2***) (3 in top flanges, webs and bottom flanges), 5 coupons were cut out in the hot rolled bottom central plate (***Pos.1***) and 10 coupons were cut out from the remaining longitudinal rebars (***Pos.4***). The tensile tests on the steel coupons were carried out at the laboratory of the University of Luxembourg according to EN ISO 6892-1 (2016). For the steel beam, two different steel grades were used for the bottom plate and for the side plates, respectively S355 and S235. The resulting mean measured yield strengths were $f_{y,cf,m}$=322 MPa for the cold-formed side plates, and $f_{y,hr,m}$=417 MPa for the hot-rolled bottom plate. The steel rebars class was B500 B, the mean measured yield strength was $f_{s,m}$=581 MPa. Compared to the steel grade ordered, the mean measured yield strengths were in accordance with EN 10025-2 (2005).

Table 1 Main dimensions of the composite section

Designation	Symbol	Values
Effective width of the composite slab	b_{eff}	1.5 m
Height of the concrete slab	h_c	72 mm
Height of the steel deck	h_p	58 mm
Area of rebars in the composite slab	$A_{s,slab}$	3.35 cm^2/m
Width of the downstand RC beam	b_{rc}	212 mm
Height of the downstand RC beam	h_{rc}	258 mm
Area of the longitudinal rebars	A_s	6.28 cm^2/m
Thickness of the central plate	t_{hr}	8 mm
Width of the central plate	b_{hr}	180 mm
Thickness of the side plates	t_{cf}	4 mm
Edge stiffeners height	c_{cf}	30 mm
Top flanges width	$b_{cf,sup}$	70 mm
Webs height	$h_{cf,w}$	270 mm
Bottom flanges width	$b_{cf,inf}$	100 mm

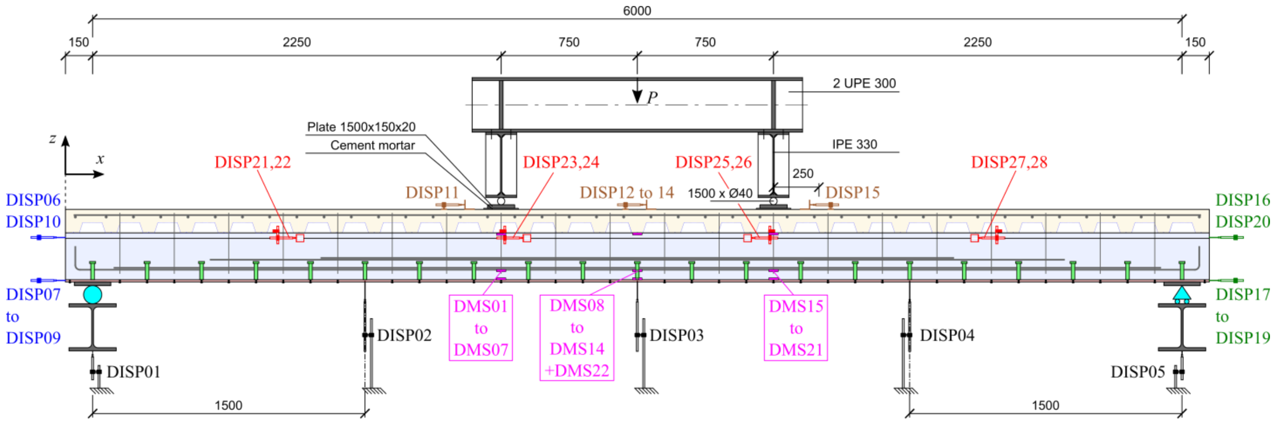

Fig. 3 The test setup and the positions of the measurements devices

2.3 Fabrication

The different steel parts were delivered separately to the Laboratory, the central plates were delivered with the shear studs already welded and the side plates were already folded in the asymmetric Z-shaped section. The steel beam assembly was done at the laboratory with self-drilling screws at the bottom of the section (instead of welding). In fact, as the side plates were already galvanized it was better to not weld them to avoid toxic smokes. Before this assembly, the three plates were carefully positioned by using clams and a timber template. In order to avoid a local plate buckling during the test, additional plates and stiffeners were welded on the beam at the position of the supports. The self-drilling screws were fixed directed towards the interior of the section. Thus, the end of the screws, which are quite long because of the drilling part, were not visible from underneath the beam. In total 164 screws were used distributed along the beam by lines of four spaced by 150 mm. For the experimental test only, the portion of the screws protruding from the plates was cut off to ensure that they would not participate in the composite connection.

The assembled steel beam was then placed in a timber formwork able to bear the two steel decks on both side of the steel beam. In a real construction, the steel decking would be supported by the developed U-shaped steel section and not by formwork or propping supports. In fact, the U-shaped steel beam is stable and resistant in construction stage. This is subject to other investigations (also experimental) and are related in Turetta *et al*. (2019). The steel decks were nailed on the top flanges of the steel beams at every steel deck rib (see Fig. 2(a)). In order to prevent a separation between the concrete slab and the downstand beam, the stirrups were linked to the wire mesh. The longitudinal rebars were assembled outside of the beam with the first half of the stirrups and then placed inside the U-shaped section (see Fig. 2(b)). The reinforcing mesh was then placed on the top of the steel decks. The second half of the stirrups was inserted to link the wire mesh to the cage composed of the first half of stirrups and the longitudinal rebars. The concrete was delivered by a local company and cast immediately. With this type of solution, the filling of the U-shaped section was done easily. The concrete was vibrated and cured carefully during two weeks.

3. Experimental test

3.1 Objectives of the test

The objectives of the flexural test conducted at the laboratory of the University of Luxembourg were to characterize the composite mechanical behavior of the studied section and therefore the efficiency of the shear connection located in tension zone.

3.2 Test setup

The test conducted at the laboratory was a 4-points bending test. The beam was on roller supports. The load was applied at 2 points, 2.250 m from the supports on each side. The loading system consisted of a main beam (2xUPE300) that spreads the force of the hydraulic jack on two transversal beams (IPE330). Under the bottom flange of these transversal beams, circular bars (15000xØ40 mm) were welded. These circular bars were in contact with plates (1500x50x20 mm) placed on the top of the composite slab. A cement mortar was inserted between these plates and the slab in order to spread the force. The maximal available force of the hydraulic jack was 1000 kN. The force and the stroke of the jack were measured throughout the test and the jack was controlled in displacement.

3.3 Instrumentation

Displacement sensors and strain gauges used during the test are described in this section. Every position of the measurement devices are represented in Figs. 3 and 4 (DISP for displacement sensors and DMS for strain gauges).

3.3.1 Displacement sensors

28 Linear Variable Differential Transducers (LVDT) were used to record the deflection, the shortening of the top of the composite slab and the slip between concrete and steel.

The deflection of the beam specimen was measured in 3 points, 1 at mid-span (DISP 03) and 2 at quarter span from each support (DISP 02 and 04). With high loads, the supporting beams had small deflections; this was also measured during the test (DISP 01 and 05).

The shortening of the concrete on top of the composite slab was measured in 5 points, 1 near each loading points (DISP 11 and 15) and 3 at mid-span (DISP 12 to 14). The ratio of the shortening on the initial distance between the points measured gives the strain on the top of the composite slab. The 3 LVDTs on the top of the slab at mid-span gives also the strain distribution within the slab width and so information on the shear lag effect.

The slip between the concrete and the steel beam was measured at both ends of the beam specimen and at 4 positions along the beam length. At each end, the end-slip was measured in 5 points at the steel-concrete interfaces (see Fig. 4). At the upper parts of the steel webs (DISP 06, 10, 16 and 20), at the lower part of the steel webs (DISP 07, 09, 17 and 19) and at the central bottom plate (DISP 08 and 18). The slip was also measured along the beam length at 1 meter from each support (DISP 21, 22, 27 and 28) and under the 2 loading points (DISP 23 to 26). In order to do so, before concreting, bars were inserted transversally to the downstand concrete beam between two steel decks ribs. On each side of the beam specimen, a pair of LVDTs was fixed to these bars and measured, during the test, the relative displacement between the bars embedded in concrete and the top flanges of the U-shaped beam (see Fig. 3).

3.3.2 Strain gauges

22 strain gauges (DMS) recorded the strains in the different steel parts of the composite beam. All the DMS were embedded in the concrete (glued before concreting). Their positions in the cross-section are presented in Fig. 1 and along the longitudinal axis in Fig. 3. The strains were measured at 3 locations, under the 2 loading points and at mid-span. At each location, the DMS were glued to the U-shaped section at five positions (DMS 01 to 05, DMS 08 to 12+22 and DMS 15 to 19) and also glued to the two lowest longitudinal rebars (DMS 06,07, DMS13,14 and DMS 20,21).

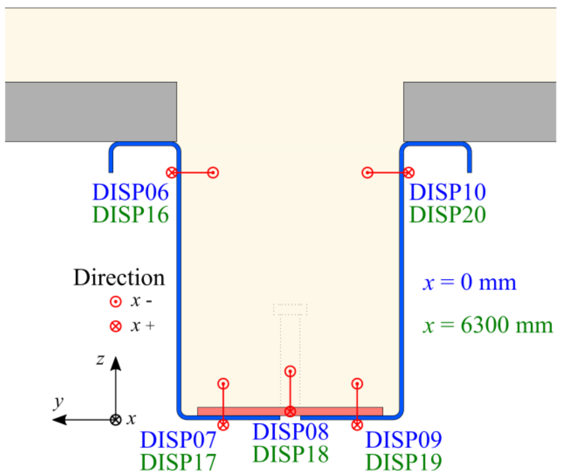

Fig. 4 Position of the LVDTs at the ends of the specimen

3.4 Test procedure

During the test; the speed rate of the jack was varying from 2 to 5 mm/min. Before the beginning of the test, the position of the beam on the supports and the position of the loading points on the composite slab were carefully checked.

The loading procedure was a quasi-static test following the recommendation of EN 1994-1-1 (2005), Annex B. The load was firstly increased to 22.5% of the predicted maximum load bearing capacity. The load was cycled 25 times between 5% and 40% of the predicted maximum capacity. After the cycles, the beam was then statically loaded. The displacement of the cylinder was increased by step-wise 4 mm gradually with a waiting time of 5 minutes to allow the relaxation of the concrete. 3 unloading were operated during the test, this gave indications on the flexural stiffness of the beam at the time of the unloading. The loading was then increased to the peak load and finally until failure, when no further load could be sustained.

3.5 Test results

3.5.1 Observations and failure mode

The 25 cycles were conducted without any apparent problem. At almost 80% of the ultimate load corresponding to the end of the linear mechanical behavior, a loud sound were heard without any visible default. The end-slip started to be visible (1-2 mm). The load kept increased until 95% of the ultimate load. Some cracks were developing in the sides of the concrete slab. The failure was finally obtained by a shear mechanism, characterized by the lifting of the composite slab in the shear span accompanied with important visible cracks on top of the slab (see Fig. 5).

At the same position, in the shear span, underneath the slab, a high opening crack appeared in the downstand concrete beam with an inclination of approximatively 45° (see Fig. 6).

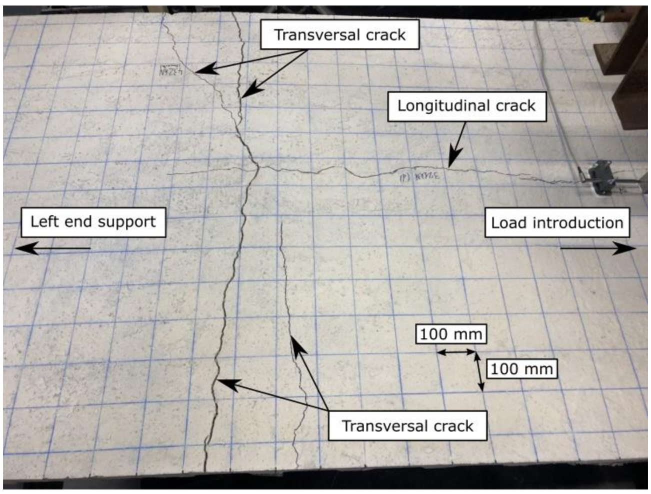

Fig. 5 Visible cracks on top of the slab at the failure

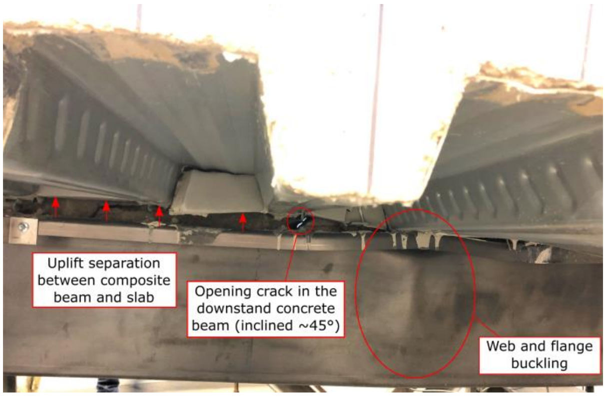

Fig. 6 Visible crack opening on the downstand concrete beam at the failure

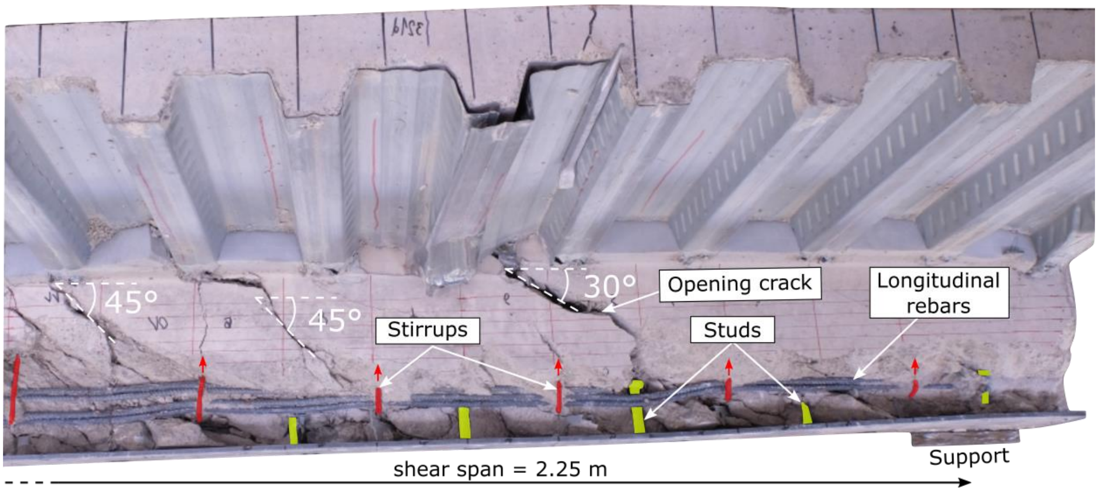

Fig. 7 The composite beam specimen after the test without the steel side plates

After the test, the side plates of the U-shaped steel section were removed from the composite beam specimen in order to investigate precisely the failure mode. The concrete severely cracked was removed manually and the rest was done carefully with a small pneumatic hammer in order to see the reinforcements and the headed studs.

In Fig. 7, it can be seen that the longitudinal reinforcement bars were bended between the stirrups, they were not straight as they were at the origin. This highlights that there was an important tension force in the stirrups and they were pulled in the direction of the composite slab. As shown in Fig. 7, the cracks in the downstand concrete beam were inclined between 30 and 45° in the shear span. This is typically relevant of a shear failure mechanism.

The concrete was removed at the opening crack and it appeared that the stirrups had failed by tension on both sides.

As it is shown in Fig. 8, it was possible to see the necking of the ductile steel reinforcement. This highlights that there was probably not enough shear resistance provided by the composite beam specimen. The failure by shear is probably increased by the presence of the headed studs transferring the longitudinal shear between the steel and the concrete parts. Without the presence of the shear studs, the failure would have been probably a slip failure between the two materials characterized by an important longitudinal slip at the steel- concrete interface. However, the presence of the shear studs increase the flexural resistance of the section as it is showed in §3.5.2 and it should be noted that this failure mechanism only appeared at very high displacements, the flexural behavior of the composite beam specimen stayed ductile until this failure.

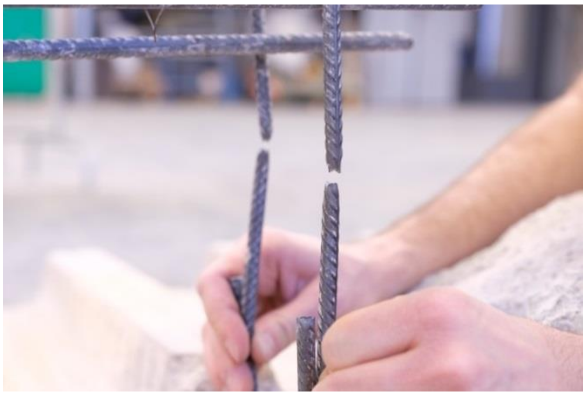

Fig. 8 Stirrups failure on both sides at the opening crack

3.5.2 Moment displacement curve

The record of the measurements data started after placing the specimen on the roller supports. Therefore, the effect of the self-weight was not taken into account in the measured values. The self-weight of the composite beam is estimated at 5.387 kN/m and the self-weight of the loading system is estimated at 2.407 kN per point load. Finally, the additional moment due to the effects of self-weight is estimated at M_{sw}=29.66 kNm and the associated deflection at δ_{sw}=1.22 mm. The moment-deflection curve represented in Fig. 9 has been adjusted to take into account these additional effects. The composite beam specimen showed a ductile behavior until the failure characterized by the drop

For $0 \le x \le 3L/8$:

$$y_1(x) = \frac{P}{2EI}\left(\frac{x^3}{6} + C_1 x + C_2\right) \tag{2}$$

For $3L/8 \le x \le 5L/8$:

$$y_2(x) = \frac{3PL}{16EI}\left(\frac{x^2}{2} + C_3 x + C_4\right) \tag{3}$$

For $5L/8 \le x \le L$:

$$y_3(x) = \frac{P}{2EI}\left(-\frac{x^3}{6} + \frac{Lx^2}{2} + C_5 x + C_6\right) \tag{4}$$

and the descending branch. The ultimate bending capacity of the composite beam tested was $M_{u,test}$=530.9 kNm, reached for a mid-span deflection of $\delta_{u,test}$=112.3 mm (L/53).

For design purpose, as the beam presented an important ductility and therefore a great plastic plateau, a pseudo-plastic resistance is estimated as already mentioned by Jaspart (1997). In this manner, 10% of the elastic stiffness (S_{el}) is retained and offset to approach the test curve as shown in Fig. 9.

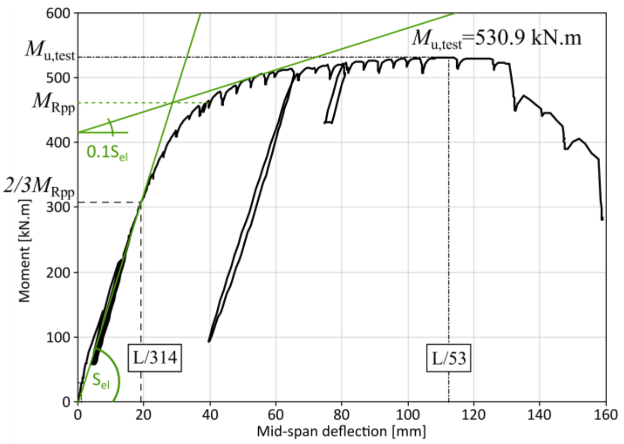

Fig. 9 Moment – deflection curve

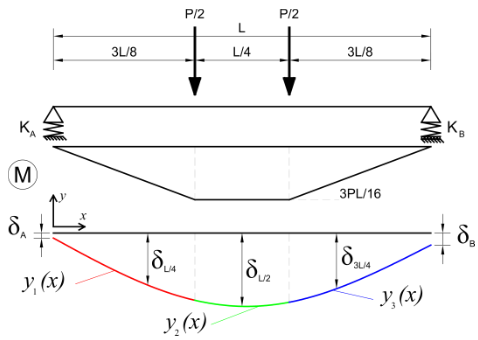

Fig. 10 Evolution of the deflection with the loading

The pseudo-plastic moment resistance is then obtained at the intersection between this line and the elastic stiffness. The pseudo-plastic moment resistance is then estimated at M_{Rpp}=461.1 kNm (87% of $M_{u,test}$). It is assumed that this resistance would be used for the design at Ultimate Limit State (ULS). The bending capacity obtained with the test clearly showed that the section behaved compositely due to the presence of the connection through the headed shear studs. Indeed, the bending resistance of the same section without connection would be divided by two. According to the combination of actions recommended in EN 1990 (2003), the loads for Serviceability Limit State (SLS) are approximately equivalent to 2/3 the ULS loads. Therefore the deflection at SLS, can be assumed at $2/3M_{Rpp}$=307.4 kNm and so $\delta_{SLS,test}$=19.1 mm (L/314). Beside the ductility, by its deflection around L/50 at failure, and the high bending capacity, this type of composite beam fulfills the common requirement of deflection limit for SLS (less deflection than L/300).

3.5.3 Flexural stiffness and deflection

The deflection of the composite specimen was measured in 3 points along the beam length ($\delta_{L/4}$, $\delta_{L/2}$ and $\delta_{3L/4}$) and at the supports (δ_A and δ_B) thanks to the displacement sensors DISP 01 to 05 (see Fig. 3). The supports presented non-negligible vertical displacement, 3 mm and 5 mm for each support at the failure load. That is why, in order to estimate the real deflection and the associated stiffness, the deflection was analytically evaluated by assuming the beam simply supported on two elastic supports with different stiffnesses (K_A and K_B) as described in Fig. 10. The analytical equations representing the deflection can be obtained by the following Eqs. (2)-(4).

With the constants

$$C_1 = \frac{-15L^2}{128} + \frac{EI}{L}\left(\frac{1}{K_A} + \frac{1}{K_B}\right), C_2 = \frac{-EI}{K_A}$$

$$C_3 = \frac{-L}{2} + \frac{8EI}{3L^2}\left(\frac{1}{K_A} + \frac{1}{K_B}\right), C_4 = \frac{3L^2}{128} - \frac{8EI}{3LK_A}$$

$$C_5 = \frac{-49L^2}{128} + \frac{EI}{L}\left(\frac{1}{K_A} + \frac{1}{K_B}\right), C_6 = \frac{19L^3}{384} - \frac{EI}{K_A}$$

Where the stiffnesses at the supports are defined by

$$K_A = \frac{P}{2\delta_A}, K_B = \frac{P}{2\delta_B}$$

It is finally possible to represent the evolution of the vertical displacement of the composite beam specimen during the test as shown in Fig. 11. The points in the figure are the real measured valued by the LVTDs and the curves are governed by the Eqs. (2)-(4). For each selected load step, it is possible to obtain the flexural stiffness of the beam by fitting the curves with the measured points; the results are presented in Table 2.

3.5.4 Slip at the steel-concrete interface

The slip was measured at the interface between steel and concrete at the ends of the composite beam (see DISP 06 to 10 and DISP 16 to 20 in Fig. 4) and along the beam length at 4 positions (see DISP 21 to 28 in Fig. 3). The evolution of the slip between the steel and concrete along the beam length is represented in Fig. 12. In this figure, the slips presented along the beam length were almost at the same height in the composite section (near the top of the steel section). That means the different points showed in Fig. 12 are the average slips at DISP06-10, DISP-21-22, DISP23-24, DISP25-26, DISP27-28 and DISP16-20.

The failure of the beam appeared on the left side this can explained why the slip recorded at the failure is more important this side. In fact, on this left side, the maximum measured slip reached 16 mm after the failure. This is not represented in Fig. 12 because this measure was affected by the failure mechanism characterized by the opening of the concrete downstand beam and the separation from the U-shaped section (see § 3.4.1).

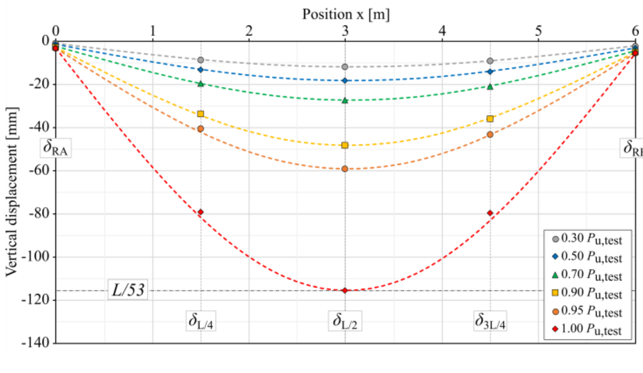

Fig. 11 Evolution of the deflection with the loading

Table 2 Estimated flexural stiffness at a load-step

Load step	P_{test} [kN]	$\delta_{L/2,test}$ [mm]		EI_{test} [MN.m^2]
0.30 $P_{u,test}$	134.82	-11.67	(L/514)	53.8
0.50 $P_{u,test}$	222.52	-18.14	(L/331)	57.4
0.70 $P_{u,test}$	311.14	-27.01	(L/222)	53.3
0.90 $P_{u,test}$	401.02	-48.15	(L/125)	37.2
0.95 $P_{u,test}$	423.15	-59.00	(L/105)	31.6
1.00 $P_{u,test}$	445.55	-115.18	(L/53)	16.5

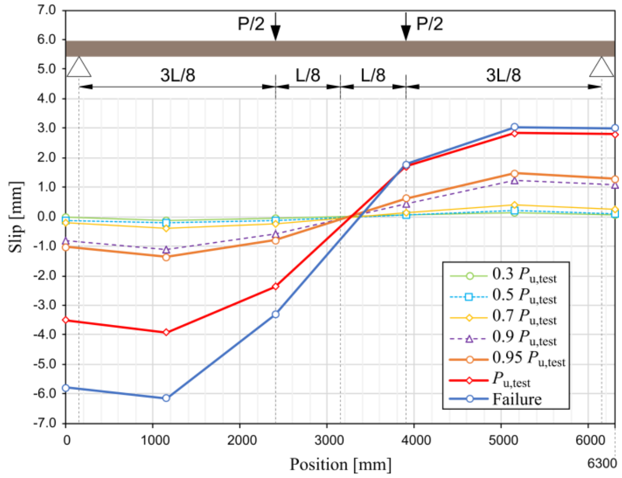

Fig. 12 Evolution of the slip along the beam with loading

(a) Headed shear stud 1 (b) Headed shear stud 2

Fig. 13 Shear studs deformations after the test

The distribution of the slip before the failure is quite symmetric around the mid-span and showed the same type of curve as for a standard composite beam.

The slip before failure, never exceeded 6 mm, which is a limit according to EN 1994-1-1 (2005) for the ductility of a shear connection. It can be concluded that there were no longitudinal slip failure between the steel and concrete. The shear connection employed with the number of headed shear studs described in § 2.1 was sufficient for the test. After the test, the bottom steel plate with shear connectors welded on it was removed from the beam specimen (see Fig. 13). The part removed was on the same side as the observed failure.

It can be seen some deformation, the first shear stud is bent with a horizontal plastic deformation of 6 mm (see Fig. 13(a)) but the second is not really yielded (see Fig. 13(b)).

This also confirms that the shear connection was sufficient and that the beam specimen behaved as a composite beam.

3.5.5 Strains

Strain gauges were placed on the steel parts in 3 cross sections along the beam, at the 2 load introduction and at mid-span (see § 3.2.2). For the concrete, displacement sensors were placed on the top of the composite slab to measure the shortening.

For fabrication facilities, the strain gauges were all embedded in the concrete, including the ones used to measure the strain in the U-shaped steel beam. As the measurements of the strains at the steel-concrete interface were perturbed during the test, probably because of the slip, it would have been better to locate the gauges outside the concrete. However, selected data can be post-treated before the peak load ($P_{\mathrm{u,test}}$). The evolution of the tensile strains with the loading, at mid-span, in the bottom central plate and in the bottom rebars are represented in Fig. 14. The evolution of the compression strain, at mid-span, in the top concrete slab is represented in Fig. 15.

The elastic limit strains for the 3 different steel parts that composed the beam specimen are estimated according to Hook's law (see Eq. (5)). For the concrete part, the compressive strain at the peak stress can be estimated by Eq. (6) according to EN 1992-1-1 (2005). The strains limits values are presented in Table 3.

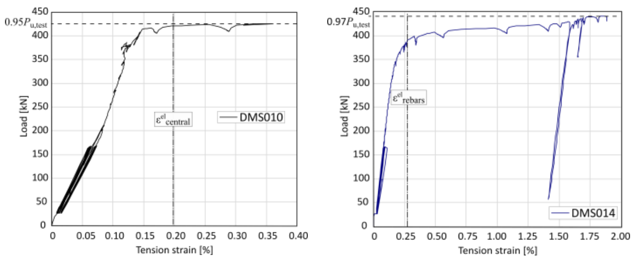

(a) In the bottom central plate (b) In the bottom rebars

Fig. 14 Evolution of the tensile strain in the steel parts at mid-span with increasing load

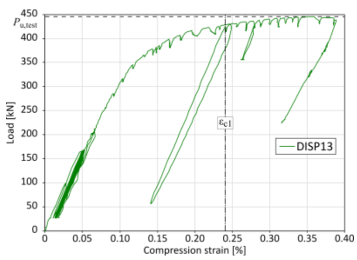

Fig. 15 Evolution of the compression strain at the top concrete slab with increasing load

Table 3 Estimated limit strains for the used materials

Material	Grade	$f_{\mathrm{y,m}}$ or $f_{\mathrm{c,m}}$ [MPa]	$\varepsilon^{\mathrm{el}}$ or $\varepsilon_{\mathrm{c1}}$ [%]
Side plates	S235	322	0.15
Central plate	S355	417	0.20
Longitudinal rebars	Fe500	581	0.28
Concrete	C35/45	53.4	0.24

According to the tensile strains measured, it can be concluded that both the steel rebars and the bottom steel plate yielded during the test. The rebars achieved a highest plastic deformation compared to the tensile strain in the bottom steel plate even if the bottom plate was closer to the overall bottom fiber of the global composite section. This underlined that there was a slip strain between the U-shaped steel beam and the reinforced concrete part. For the concrete, the limit strain ($\varepsilon_{\mathrm{c1}}$), estimated by the shortening of the displacement sensors, seems to be exceeded near the peak load.

$$\varepsilon^{el} = f_{\mathrm{y,m}} / E \tag{5}$$

$$\varepsilon_{c1} = 0.7\, f_{\mathrm{c,m}}^{0.31} \tag{6}$$

From the strain values measured in the top and bottom fibers of the composite section, the strain distribution with the loading in the composite beam is represented in Fig. 16.

For a better readability, the strain distribution in Fig 16 is separated in two parts: in the reinforced concrete part (a) and in the U-shaped steel beam (b). For the reinforced concrete part (see Fig 16 (a)), the Elastic Neutral Axis (ENA) is located near the top of the steel beam until $0.8P_{\mathrm{u,test}}$. With higher loading (like $0.95P_{\mathrm{u,test}}$), due to the yielding of the bottom longitudinal steel rebars, the neutral axis is moving to an Elasto-Plastic Neutral Axis (EPNA) located in the composite slab. For the U-shaped steel part (see Fig 16 (b)), every parts were in tension.

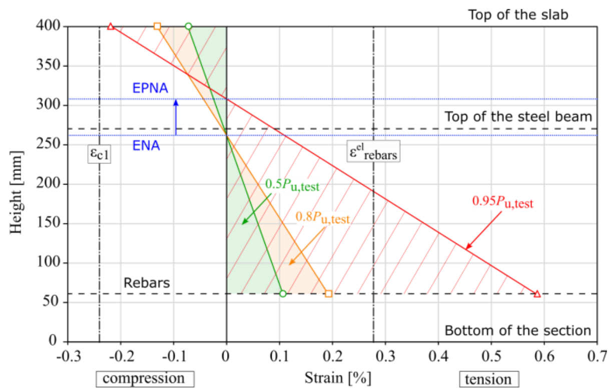

(a)

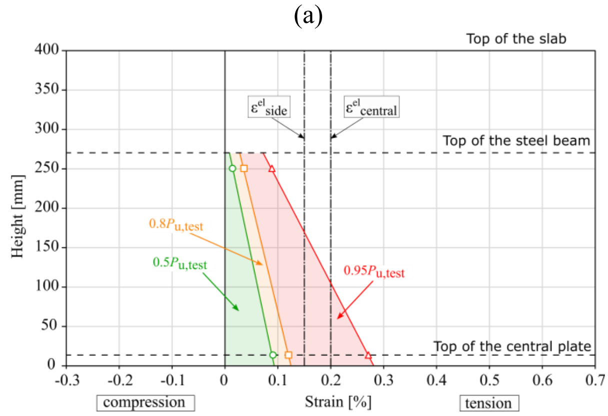

(b)

Fig. 16 Strain distribution in the composite section at different load steps, (a) in the reinforced concrete part and (b) in the U-shaped steel parts

4. Analytical study

4.1 Analytical evaluation of the bending resistance by integrating the stress distribution

The bending resistance moment is firstly evaluated by integrating the stress distribution obtained from the strain distribution shown in Fig. 16 at $0.95P_{\mathrm{u,test}}$ which corresponds almost to the ultimate resistance of the section.

It is assumed that after exceeding the yield strain of a steel part (see Table 3), the resulting stress is the yield strength of the material without taking into account strength hardening. This assumption is the same as for a full plastic analysis according to EN 1994-1-1 (2003). For instance, with this assumption, when looking at the distribution of the strain in the steel side plates (see Fig 16(b)), the yield strain was exceeded in all bottom fibers, on a height of 164 mm. This is resulting in a constant stress block for the side plates until this height (see Fig. 17). For the rest of the steel part, the stresses are assumed to be proportional to the strains, the elastic stresses values ($\sigma_{\mathrm{a,i}}$) are directly obtained by Hook's law (see Eq. (5)) from the strain values ($\varepsilon_{\mathrm{a,i}}$) measured during the test (with DMS) and represented in Fig. 16(b).

For the concrete, only a rough estimation of the strains could be extracted from the measurements at the top of the concrete slab (with LVTD). Therefore, the stress values where not obtained directly from the measured values of the slab deformation but by solving the horizontal equilibrium between resulting tension and compression forces integrated from the stress distribution of the steel parts (see Fig. 17). The stress distribution in the concrete slab was assumed linear from the EPNA to the top of the slab. The maximum stress in concrete was thus obtained at $\sigma_{\mathrm{c,1}}$=23.4 MPa, it was far from the concrete strength from compression tests ($f_{c\mathrm{,m}}$=53 MPa, see § 2.2), the approximation of a linear distribution of the stress in the concrete slab is then acceptable.

Finally, the elasto-plastic bending resistance of the tested composite specimen, at $0.95P_{\mathrm{u,test}}$, is assessed at $M_{\mathrm{epl,R}}$=471.1 kNm by integrating the stress distribution presented in Fig. 17 with Eq. (10).

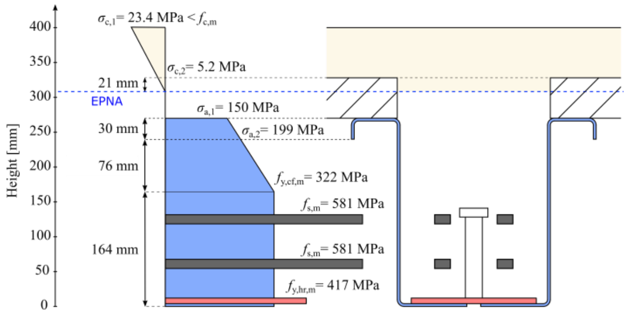

Fig. 17 Elasto-plastic stress distribution in the composite section at $0.95P_{\mathrm{u,test}}$

The associated applied moment during the test was $M_{0.95\mathrm{,u,test}}$=504.4 kNm. Compared to the test results the elasto-plastic bending resistance moment is 6.6% inferior to the applied bending during the test. Additionally, the assessment is also based on the location of the EPNA, which has been assessed roughly from only 2 points (see Fig. 16(a)). However, the distribution of the stress underlined well that the cold-formed side plates were not entirely yielded.

$$M_{\mathrm{epl,R}} = \int_S z_i \sigma_i dS \tag{10}$$

4.2 Plastic bending resistance limited by the available shear capacity of the composite connection

The elasto-plastic bending resistance determined in § 4.1 was based on the evaluation of the real distribution of stresses in the composite section. However, the method is not convenient for a design calculation because it needs the assessment of the strains in the composite section. Therefore, a simplified approach is proposed in this paragraph.

The proposed method takes into account the yielded parts of the steel plates, as it was the case in § 4.1, but neglects the steel parts subjected to an elastic stress distribution.

The shear connection is partial as the maximal available shear force that the connection can transfer ($V_{\mathrm{l,max}}$), calculated by Eq. (11), is lower than the minimal value of the compression stress resultant in the concrete (N_{c}) and the tension stress resultant in the steel section (N_{a}).

It is thus suggested to determine the area of the yielded steel limited by the available shear capacity of the connection ($V_{\mathrm{l,max}}$=907.3 kN) obtained by Eq. (11).

$$V_{\mathrm{l,max}} = N_{\mathrm{sc}} P_R \tag{11}$$

$$P_R = 0.8 f_{\mathrm{u}} \pi d_{sc}{}^2 / 4 \tag{12}$$

In Eq. (11), N_{sc} represents the number of connectors located on the shear span, between the end support and the point load (N_{sc}=8). According to EN 1994-1-1(2005), the shear resistance of a single connector (P_{R}=113.4 kN) is calculated with Eq. (12), as it is limited here by the stud failure mechanism, without considering the partial factor (γ_{V}). The ultimate tensile strength of the material of the stud (f_{u}) was taken to 500 MPa.

As underlined by the test, the steel located at the bottom of the section yielded first. Considering the yielding of the central plate, the stress resultant is given by Eq. (13) with $N_{\mathrm{a,hr}}$=600.48 kN. Since the shear capacity of the connection ($V_{\mathrm{l,max}}$) is greater than this value, a remaining force ($V_{\mathrm{l,cf}}$) can be transferred to the cold-formed side plates (see Eq. (14)). Finally, the yielded area of the cold formed side plates ($A_{\mathrm{cf,pl}}$) is determined by Eq. (15).

$$N_{\mathrm{a,hr}} = t_{\mathrm{hr}} b_{\mathrm{hr}} f_{\mathrm{y,m,hr}} \tag{13}$$

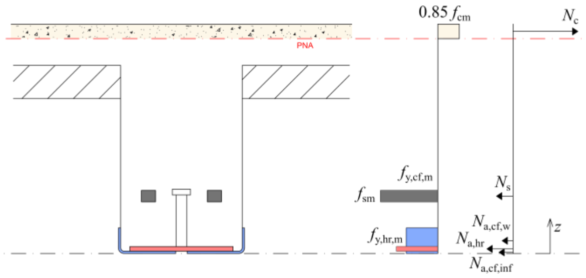

Fig. 18 Plastic stress distribution in the composite section considering only the available shear connection

Table 4 Calculation of the bending resistance with cold-formed side plates partially yielded

Composite parts	$z_{i/v'}$ [mm]	$N_{pl,i}$ [kN]	$M_{pl,R,i}$ [kNm]
Concrete in compression	391	1272.35	497.05
Longitudinal rebars	100	-365.05	-36.51
Cold-formed side webs	19	-74.97	-1.39
Hot rolled central plate	8	-600.48	-4.80
Cold-formed bottom flanges	2	-231.84	-0.46
Sum :		**0**	**453.9**

$$V_{l,cf} = V_{l,max} - N_{a,hr} \quad (14)$$

$$A_{cf,pl} = \frac{V_{l,cf}}{f_{y,m,cf}} \quad (15)$$

Where t_{hr}, b_{hr}, $f_{y,m,hr}$ and $f_{y,m,cf}$ are given in § 2.1 and 2.2.

The equilibrium between the stress resultant of the composite parts is made to find the stress block repartition of the concrete slab and the location of the PNA (see Fig. 18).

Finally the plastic bending resistance is obtained to $M_{pl,R}$=453.9 kNm (see Table 4). Compared to the test results the plastic bending resistance obtained with this method of design is 1.6% inferior to the pseudo-plastic bending resistance (M_{Rpp}=461.1 kNm, see § 3.4.2) and 14.5% inferior to the ultimate bending capacity of the composite section ($M_{ult,test}$=530.9 kNm, see § 3.4.2).

5. Conclusions

The experimental test and the analytical study carried out on this innovative U-shaped steel-concrete composite beam leads to the following conclusions:

- The developed composite beam achieved high ductility (up to L/53). The bending capacity (M_{Rpp}=461.1 kNm) was highly improved by composite action about 2.2 times compared to the same beam without connection.
- The composite connection located in the tension zone, where the concrete is potentially cracked, worked effectively.
- At very high displacement, the specimen exhibited a shear failure in the reinforced concrete part. In order to control this failure mode, for practical recommendations, it is suggested to not consider the shear resistance of the steel side plates of the U-shaped section in the calculation of the shear resistance of the composite beam. Then, this will conduct to a higher amount of stirrups participating in the shear resistance of the composite beam.
- In partial shear connection, the side plates of the steel U-shaped section partially yielded. Therefore, for the design calculation of the plastic bending resistance, it is proposed to consider the participating yielded parts with the maximum available shear force the connection can transfer to the steel section and to neglect the rest of the steel section. Combined to the EN 1994-1-1, the calculation agrees well with the test result.

Acknowledgments

This test took place in the framework of the "COMINO" PhD research project (CIFRE grant 2017/0048) in partnership with CTICM, University of Lorraine and University of Luxembourg.

The steel sections were supplied by the company BRIAND. The steel fasteners were supplied by the company HILTI. Their supports are gratefully acknowledged as well as the work made by the team of the laboratory of structural engineering of the University of Luxembourg.

However, the conclusions and recommendations presented in this article are independent and do not necessarily reflect the views of the sponsors.

References

Ahn, H.J. and Ryu, S.H. (2007), "Experimental study on flexural strength of modular composite profile beams", *Steel Compos. Struct.*, **7**(1), 71-85. http://dx.doi.org/10.12989/scs.2007.7.1.071

Ahn, H.J. and Ryu, S.H. (2008), "Experimental study on flexural strength of reinforced modular composite profiled beams", *Steel Compos. Struct.*, **8**(4), 313-328. http://dx.doi.org/10.12989/scs.2008.8.4.313

Braun, M., Obiala, R. and Odenbreit, C. (2015), "Analyses of the loadbearing behavior of deep-embedded concrete dowels, CoSFB", *Steel Construction*, **8**(3), 167-173. https://doi.org/10.1002/stco.201510024

Chen, L.H., Li, S.T., Zhang, H.Y. and Wu, X.F. (2018), "Experimental study on mechanical performance of checkered steel-encased concrete composite beam", *J. Constr. Steel Res.*, **143**, 223-232. https://doi.org/10.1016/j.jcsr.2017.12.021

EN 10025-2 (2005), Hot rolled products of structural steels - Part 2: Technical delivery conditions for non-alloy structural steels, European Committee for Standardisation (CEN); Brussels, Belgium.

EN 12390-3 (2012), Testing hardened concrete. Part 3: Compressive strength of test specimens, European Committee

for Standardisation (CEN); Brussels, Belgium.
EN 1990 (2003), Eurocode 0: Basis of structural design, European Committee for Standardisation (CEN); Brussels, Belgium.
EN 1992-1-1 (2005), Eurocode 2: Design of concrete structures. Part 1.1: General rules and rules for buildings, European Committee for Standardisation (CEN); Brussels, Belgium.
EN 1994-1-1 (2005), Eurocode 4: Design of composite steel and concrete structures. Part 1.1: General rules and rules for buildings, European Committee for Standardisation (CEN); Brussels, Belgium.
EN ISO 6892-1 (2016), Metallic materials - Tensile testing. Part 1: Method of test at room temperature, International Organization for Standardization (ISO); Geneva, Switzerland.
Goble, G.G. (1968), "Shear strength of thin flange composite specimens", *Engineering Journal, American Institute of Steel Construction*, **5**, 62-65.
Jaspart, J.P. (1997), "Recent advances in the field of steel joints - Column bases and further configurations for beam-to-column joints and beam splices", Professorship Thesis, University of Liège, Belgium.
Keo, P., Lepourry, C., Somja, H. and Palas, F. (2018), "Behavior of a new shear connector for U-shaped steel-concrete hybrid beams", *J. Constr. Steel Res.*, **145**, 153-166. https://doi.org/10.1016/j.jcsr.2018.01.028
Kim, S.H. and Aboutaha, R.S. (2004), "Ductility of carbon fiber-reinforced polymer (CFRP) strengthened reinforced concrete beam: Experimental investigation", *Steel Compos. Struct.*, **4**(5), 333-353. http://dx.doi.org/10.12989/scs.2004.4.5.333
Kozma, A., Odenbreit, C., Braun, M.V., Veljkovic, M. and Nijgh, M.P. (2019), "Push-out tests on demountable shear connectors of steel-concrete composite structures", *Structures*, https://doi.org/10.1016/j.istruc.2019.05.011
Lawson, R.M. and Taufiq, H. (2019), "Partial shear connection in light steel composite beams", *J. Constr. Steel Res.*, **154**, 55-66. https://doi.org/10.1016/j.jcsr.2018.11.005
Liu, J., Zhao, Y., Chen, Y.F., Xu, S. and Yang, Y. (2018), "Flexural behavior of rebar truss stiffened cold-formed U-shaped steel-concrete composite beams", *J. Constr. Steel Res.*, **150**, 175-185. https://doi.org/10.1016/j.jcsr.2018.08.011
Liu, Y., Guo, L., Qu, B. and Zhang, S. (2017), "Experimental investigation on the flexural behavior of steel-concrete composite beams with U-shaped steel girders and angle connectors", *Eng. Struct.*, **131**, 492-502. https://doi.org/10.1016/j.engstruct.2016.10.037
Oehlers, D.J. (1993), "Composite profiled beams", *J. Struct. Eng.*, **119**(4), 1085-1100. https://doi.org/10.1061/(ASCE)0733-9445(1993)119:4(1085)
Oehlers, D.J. and Bradford, M.A. (1995), Composite Steel and Concrete Structural Members, Pergamon, Oxford, United Kingdom.
Peng, M. and Shi, Z. (2004), "Interface characteristics of RC beams strengthened with FRP plate", *Struct. Eng. Mech.*, **18**(3), 315-330. http://dx.doi.org/10.12989/sem.2004.18.3.315
Ryu, S-H. (2010), "Study on behavior of T-section modular composite profiled beams", *Steel Compos. Struct.*, **10**(5), 457-473. http://dx.doi.org/10.12989/scs.2010.10.5.457
Turetta, M., Odenbreit, C., Khelil, A. and Martin, P.O. (2019), "Investigations on the lateral-torsional buckling of an innovative U-shaped steel beam", *J. Constr. Steel Res.*, *(Under Review)*
Uy, B. and Bradford, M.A. (1995a), "Ductility of profiled composite beams. Part I: experimental study", *J. Struct. Eng.*, **121**(5), 876-882. https://doi.org/10.1061/(ASCE)0733-9445(1995)121:5(876)
Uy, B. and Bradford, M.A. (1995b), "Ductility of profiled composite beams. Part II: analytical study", *J. Struct. Eng.*, **121**(5), 883-889. https://doi.org/10.1061/(ASCE)0733-9445(1995)121:5(883)
Zhou, X., Zhao, Y., Liu, J., Chen, Y.F. and Yang, Y. (2019), "Bending experiment on a novel configuration of cold-formed U-shaped steel-concrete composite beams", *Eng. Struct.*, **180**, 124-133. https://doi.org/10.1016/j.engstruct.2018.11.001

BU